ADVANCED ENERGY MATERIALS
www.advenergymat.de

A Comparative Study of Redox Mediators for Improved Performance of Li–Oxygen Batteries

Chengji Zhang, Naveen Dandu, Sina Rastegar, Saurabh N. Misal, Zahra Hemmat, Anh T. Ngo, Larry A. Curtiss, and Amin Salehi-Khojin**

Redox meditators (RMs) are soluble catalysts located in an electrolyte that can improve the energy efficiency (reduced overpotential) and cyclability of Li–oxygen ($Li–O_2$) batteries. In this work, 20 RMs within a $Li–O_2$ system with dimethyl sulfoxide and tetraethylene glycol dimethyl ether electrolytes are studied and their electrochemical features such as redox potential, the separation of cathodic and anodic peaks, and their current intensities are measured using cyclic voltammetry (CV) experiments. Six RMs are selected as "primary" choices based on their electrochemical performance, and stability tests are then performed to examine their electrochemical responses after consecutive cycles. Moreover, galvanostatic cycling tests are performed within a $Li–O_2$ battery system assembled with selected six RMs for real case consistency investigations. It is found that results from CV to galvanostatic cycling tests are consistent for halides and organometallic RMs, where the former exhibit much higher stability. However, the organic RMs show high reversibility in CV but low in battery cycling results. Density functional theory calculations are carried out to gain more understanding of the stability and redox potentials of the RMs. This study provides comparative information to select the most reliable RMs for $Li–O_2$ batteries along with new fundamental understanding of their electrochemical activity and stability.

1. Introduction

The electrification of transportation is well-recognized as a promising strategy to minimize the dependence on fossil fuels and eventually address the concerns with climate change. Among all strong candidates for the next-generation energy storage technology, the lithium–oxygen ($Li–O_2$) battery has attracted exclusive attention due to its high theoretical energy density.[1–3] However, there are major issues with the existing $Li–O_2$ systems including degradation of the anode electrode, clogging of the cathode, electrolyte instability, and high charge overpotential.[4–6] In our previous work, we demonstrated a $Li–O_2$ battery that operates up to 700 cycles in an air-like atmosphere without any evidence of anode, cathode, and electrolyte failure.[7] Yet, the high charge potential (>4.0 V vs Li/Li^+) for the decomposition of discharge product (i.e., Li_2O_2) has remained one of the key obstacles for the practical development of the existing $Li–O_2$ systems.[8–10]

While solid catalysts have been the subject of much study for catalyzing the decomposition of discharge products,[7,11–19] recent studies have reported investigations of liquid catalysts based on redox mediators. These studies have shown that redox mediators (RMs) can effectively decompose Li_2O_2 regardless of their size, shape, or thickness, and thereby can improve the energy efficiency (reduced polarization gap) and cyclability of $Li–O_2$ batteries.[20–24] The overall reaction mechanisms of RMs are summarized in Equations (1) and (2). During charging of batteries, the RM initially gets oxidized to its higher oxidation state (Equation (1)). The oxidized form of RM (RM*) then gets involved in oxidizing the discharge product (Li_2O_2) to form Li^+ and molecular oxygen (O_2).

$$RM \rightarrow RM^* + e^- \quad (1)$$

$$Li_2O_2 + RM^* \rightarrow O_2 + 2Li^+ + RM \quad (2)$$

Thus far, RMs such as tetrathiafulvalene (TTF),[25] the I_3^-/I_2 or I^-/I_3^- from lithium iodide (LiI),[26–28] tris[4-(diethylamino) phenyl]amine (TDPA),[29] 2,2,6,6-tetramethylpiperidinyloxyl (TEMPO),[30] iron(II) phthalocyanine (FePc),[31] 2-azaadamantane-*N*-oxyl (AZADO),[32] and ferrocene (FC)[33] in either or both dimethyl sulfoxide (DMSO) and tetraethylene glycol dimethyl ether (TEGDME) have been reported by various groups. However, none of these studies have systematically investigated the performance of RMs in one specific $Li–O_2$ battery system. In

C. Zhang, S. Rastegar, S. N. Misal, Z. Hemmat, Prof. A. Salehi-Khojin
Department of Mechanical and Industrial Engineering
University of Illinois at Chicago
Chicago, IL 60607, USA
E-mail: salehikh@uic.edu

C. Zhang, Dr. N. Dandu, Dr. A. T. Ngo, Dr. L. A. Curtiss
Materials Science Division
Argonne National Laboratory
Argonne, IL 60439, USA
E-mail: curtiss@anl.gov

Dr. A. T. Ngo
Department of Chemical Engineering
University of Illinois at Chicago
Chicago, IL 60608, USA

The ORCID identification number(s) for the author(s) of this article can be found under https://doi.org/10.1002/aenm.202000201.

DOI: 10.1002/aenm.202000201

this study, from cyclic voltammetry (CV), we have examined the performance of a wide range of RMs from organometallics, halides, and organic groups (defined and categorized in Table S1 in the Supporting Information) in both DMSO and TEGDME electrolytes in terms of their electrochemical characteristics such as redox potential, separation of cathodic and anodic peaks and their current intensities. These measured CV parameters were first used to prescreen the "primary" RMs among all studied RMs. The selected "primary" RMs were then further studied regarding their reversibility from both CV and battery cycling experiments followed by density functional theory (DFT) calculation to provide insight into their stability in Li–O_2 batteries.

2. Results and Discussion

2.1. Integrated CV Results

Figure 1a shows a typical cyclic voltammogram of oxidation–reduction with FC as a redox mediator. The oxidation reaction happens toward higher potentials to obtain the anodic peak current ($I_{p,a}$) and its corresponding oxidation potential ($E_{p,a}$). Normally, the $I_{p,a}$ is given at the potential that all analytes near the surface of electrode are oxidized. After reaching its upper limit of the potential window, the potential is scanned toward a lower value until it reaches the lower limit. This reverse scan allows the cathodic peak current ($I_{p,c}$) and reduction potential ($E_{p,c}$) to appear.[34,35] In principle, the performance of RMs for Li–O_2 batteries is determined by two measures; i) the formal reduction potential (also known as redox potential, E_0), which corresponds to the level that the charge potential could be reduced. E_0 is calculated from the average of the cathodic and anodic potential, $E_0 = (E_{p,a} + E_{p,c})/2$, and ii) the electrochemical reversibility and stability of RMs that determine the long-effectiveness for the electrocatalysis and can be measured by the peak-to-peak separation, $\Delta E_p = E_{p,a} - E_{p,c}$, and peak current ratio, calculated by $|I_{p,a}/I_{p,c}|$. Small voltage gaps between cathodic and anodic potentials could reduce the possibility of RM decomposition during the battery operation.[4,36] Moreover, a preferred RM with high reversibility should ideally have a peak current ratio as close as 1.[34] In our analyses, for those analytes that reveal more than one oxidation or reduction peaks within the tested range, the first oxidation peak and correlated reduction peak were used.

Figure 1b–e shows the measured parameters for all the tested RMs in 1 M lithium bis(trifluoromethanesulfonyl)imide (LiTFSI) with DMSO electrolyte. In Figure 1b, tested RMs were arranged according to their redox potentials from low to high. We found that several nonhalide RMs such as TDPA and TMPD exhibit lower redox potential than the most common RMs such as LiI. Moreover, our results for peak-to-peak separation, ΔE_p (shown in Figure 1c) indicate that more than 70% of tested RMs, such as TDPA, TEMPO, etc., have ΔE_p in the range from 0.05 to 0.12 V (within the dashed window in Figure 1c). From the same figure, it is noticeable that ΔE_p values became larger in oxygen-rich electrolytes than those in oxygen-free electrolytes for both halide RMs (LiI and LiBr). While for the organic and organometallic (nonhalide) RMs, ΔE_p values are similar for with or without oxygen in the system except for

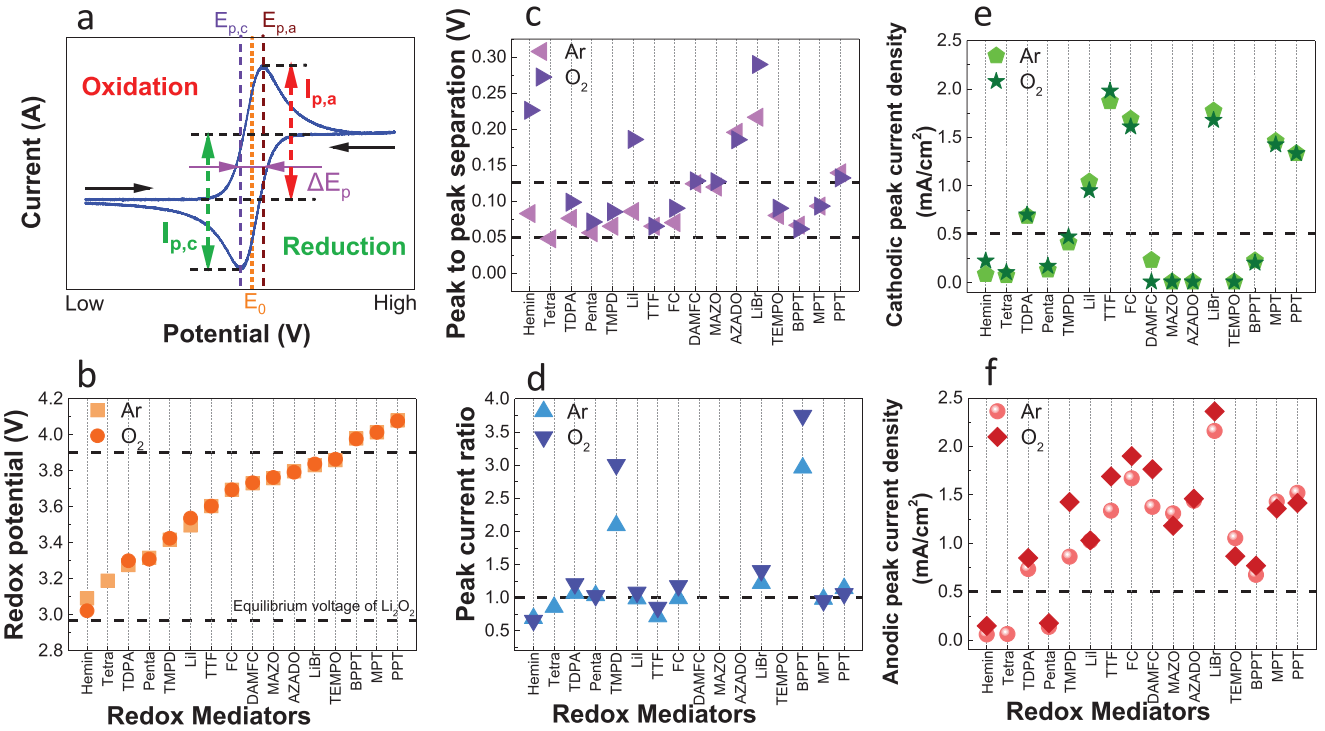

Figure 1. The electrochemical performances of tested RMs in DMSO solvent; a) schematic CV results, b) measured redox potentials, c) peak-to-peak separations, ΔE_p, d) peak current ratios, $|I_{p,a}/I_{p,c}|$, e) cathodic peak currents, $I_{p,c}$, and f) anodic peak currents, $I_{p,a}$. Some RMs like PcCo do not give any valuable electrochemical responses, thus are not plotted in this figure.

Hemin. Figure 1d also shows all tested current peak ratios, $|I_{p,a}/I_{p,c}|$. From the CV results, we found half of the tested RMs such as TDPA have their $|I_{p,a}/I_{p,c}|$ close to one (see dash line in Figure 1d), whereas RMs such as AZADO have this ratio much greater than one and RMs such as Hemin show values less than one. Figure 1e,f gives information about both cathodic and anodic peak current densities, respectively. Our results indicate that most RMs with redox potentials lower than that of LiI exhibit $I_{p,a}$ and $I_{p,c}$ values <0.5 mA cm^{-2}, which are considered to be too small for efficient oxidation of Li_2O_2. However, 80% of the measured RMs have their anodic current peaks higher than 0.5 mA cm^{-2} and 60% possess cathodic current peaks higher than 0.5 mA cm^{-2} (dashed line in Figure 1e,f).

Based on information obtained from Figure 1b–f, we selected a total of 6 "primary" RMs for further reversibility study. Selected RMs are as follows: FC group from organometallics (FC, DAMFC), LiBr and LiI from halides, and TTF, TMPD from organic RMs. These selected RMs have the following characteristics: 1) their redox potential is higher than the equilibrium voltage of Li_2O_2 and lower than the redox potential of 3.9 V. 2) In terms of electrochemical stability, for peak-to-peak separation, ΔE_p, we selected a range from 0.05 to 0.12 V (in between the dashed lines in Figure 1c) as most of tested RMs fall in this range; for current peak ratios, $|I_{p,a}/I_{p,c}|$, we selected RMs to have it one or near one (dashed line near Figure 1d); when selecting from the anodic and cathodic peak current intensity, the limit was set to be at 0.5 mA cm^{-2} or above. 3) They are highly soluble in the selected solvents (e.g., DMSO and TEGDME). 4) They do not get decomposed easily when attacked by oxygen radicals or anions such as superoxide or peroxide moieties formed during oxygen reduction reaction (ORR) and oxygen evolution reaction.[20,37,38] Compared to selected preferred RMs, other RMs have either one or more factors that are not satisfied with the listed requirements. For example, 10-isopropylphenothiazine (PPT) and its radical groups show redox potentials above 4.0 V, which increases the possibility of getting destabilized at higher cycles; FePc from organometallics and 5,10,15,20-tetraphenyl-21*H*,23*H*-porphine iron(III) chloride (Tetra) have low solubility (<2 × 10^{-3} M); AZADO and its radical 1-methyl-2-azaadamantane-*N*-oxyl (MAZO) show sharp oxidation current peaks with decent redox potentials, but lack of reduction peaks give an exorbitant $I_{p,a}/I_{p,c}$ ratio.

2.2. CV Reversibility Test

Figure 2 shows the CV reversibility results for the selected "primary" RMs tested in DMSO electrolyte. First, we observe negligible intensity loss from 1st to 40th cycle for both halide RMs (shown in Figure 2a,b). This justifies the stability of redox couples of X^-/X_3^- and X_3^-/X_2 with consecutive cycles (X = Br, I). While both halide RMs exhibit superb stabilities, organometallic RMs such as DAMFC and FC (shown in Figure 2c,d) lose nearly half of their voltammetric currents during oxidation. Organic RMs also show differentiated results from the overall stable TTF (90% intensity after 40 cycles; Figure 2e) to TMPD (30% intensity after 40 cycles; Figure 2f). The stability for tested RMs follows the order of halides > organics > organometallics.

Additionally, CV experiments were performed using TEGDME as a solvent with the same RMs to screen for the solvent effect (**Figure 3**). Comparing Figures 2 and 3, we first noticed the CV patterns obtained from TEGDME electrolyte are different than those of DMSO electrolyte. Both organometallic RMs and LiBr from halide group (Figure 3b–d) show

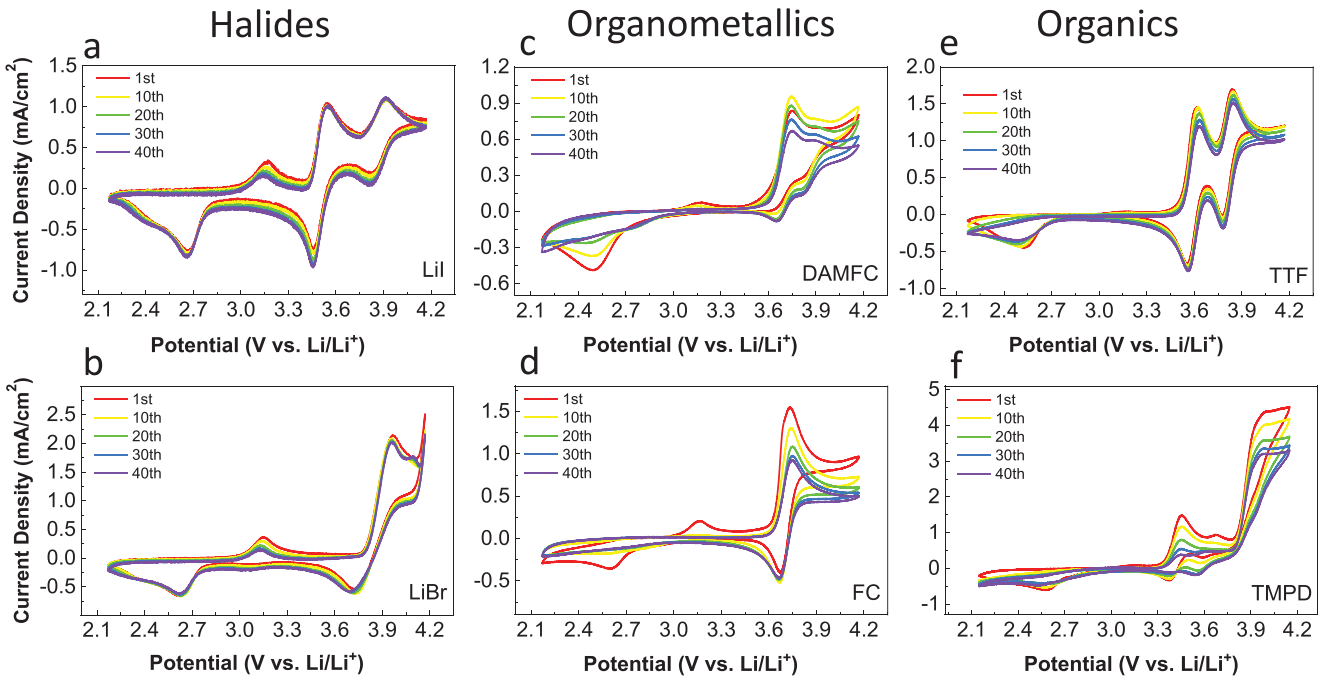

Figure 2. CV result for electrochemical reversibility test from selected "primary" RMs, which dissolved in 1 M LiTFSI in DMSO. They are a) LiI and b) LiBr from halides, c) DAMFC and d) FC from organometallics, and e) TTF and f) TMPD from organics. All the electrolyte was prepurged with O_2 before the test; sweep rate was controlled at 10 mV s^{-1}.

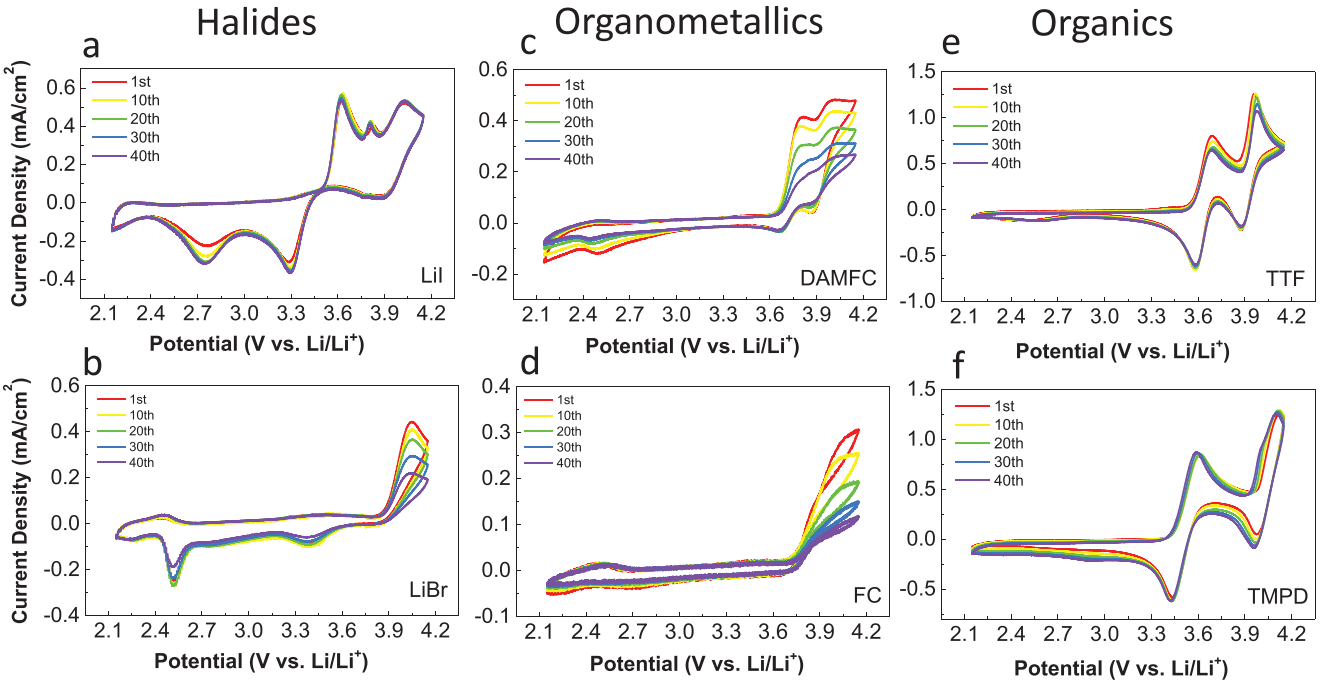

Figure 3. CV results for electrochemical reversibility test of the same selected RMs with 1 M LiTFSI in TEGDME. They are a) LiI and b) LiBr from halides, c) DAMFC and d) FC from organometallics, and e) TTF and f) TMPD from organics. All the electrolyte was prepurged with O_2 before the test; sweep rate was controlled at 10 mV s^{-1}.

less reversibility for TEGDME compared to DMSO. Moreover, in TEGDME, we observed drastically weakened reduction peak current for these RMs. For organic RMs, TTF kept its overall electrochemical configuration in both DMSO and TEGDME (Figure 3e), whereas TMPD revealed better reversibility in TEGDME than in DMSO (Figure 3f). Apart from the reversibility, it is noteworthy to mention that the voltammetric potential of the first anodic peak of most tested RMs in TEGDME were shifted to a more positive potential than that in DMSO electrolyte. For LiBr (also shown in Figure S3 in the Supporting Information), the first oxidation potential of Br^-/Br_3^- happens at 3.97 V in DMSO, where the same oxidation potential revealed at 4.05 V in TEGDME electrolyte. In terms of current intensity, the first oxidation and reduction peak currents were reduced in case of TEGDME, compared to DMSO, from 2.4 and 0.4 to 0.4 and 0.1 mA cm^{-2}, respectively.

2.3. Galvanostatic Cycling Test

Next, the six selected RMs were tested within the Swagelok Li–O_2 battery cell for 50 cycles first with DMSO electrolyte. Results are shown in **Figure 4**. We observed that the RMs (e.g., TMPD and LiI) with lower redox potentials (3.30–3.60 V vs Li/Li^+) exhibit lower charge potentials than those RMs (e.g., FC and LiBr) with greater (3.60 V vs Li/Li^+) redox potential. For example, TMPD (shown in Figure 4f) with a redox potential of 3.43 V revealed a 3.3 V of charge potential, yet LiBr (shown in Figure 4b) with a redox potential of 3.84 V showed a charge potential of 3.75 V. These results further support the selection of RMs that possess closer redox potentials to the oxidation potential of Li_2O_2. Based on battery cycling results, halide RMs (Figure 4a,b) exhibit the best stability among all three types of RMs since the charging potential remains almost constant at 3.4 V for LiI and 3.8 V for LiBr. This is consistent with our DFT results that the halide radicals are stable with respect to singlet oxygen (see below). For organometallic RMs (shown in Figure 4c,d), even though FC showed the best electrochemical reversibility in terms of its ΔE_p and $|I_{p,a}/I_{p,c}|$, the anodic current intensity decreased drastically during CV stability test in both DMSO and TEGDME. This trend is further justified from the battery cycling test, as FC only offered 10 mediated cycles where its charge potential gradually increased from 3.6 to 4.1 V, which is considered as noncatalyzed potential for a Li–O_2 battery.[39,40] Our results indicate that both organometallic RMs are not preferred to work solely as RM for catalyzing Li–O_2 battery. For organic RMs such as TTF or TMPD, even though they showed remarkable chemical characteristics and stabilities in CV reversibility test, their galvanostatic cycling results revealed a different trend. At its earliest stage (1st cycle), superb effectiveness was observed for reducing charge potential using both TTF (3.5 V; shown in Figure 4e) and TMPD (3.3 V; shown in Figure 4f). However, charge potentials keep increasing after each cycle, approaching the nonmediated charge potential region (>4.1 V). The deactivation of organic or organometallic RMs is likely resulting from the interactions between the singlet oxygen produced during oxygen reduction reaction and those methyl groups that are next to O or N atoms of RMs.[37,41,42]

Like DMSO, in TEGDME electrolyte, our battery results (shown in **Figure 5**) show smaller charge potentials at the initial stage (1st cycle). For organic RMs like TMPD and TTF, the overall curve features also remain similar in both electrolytes.

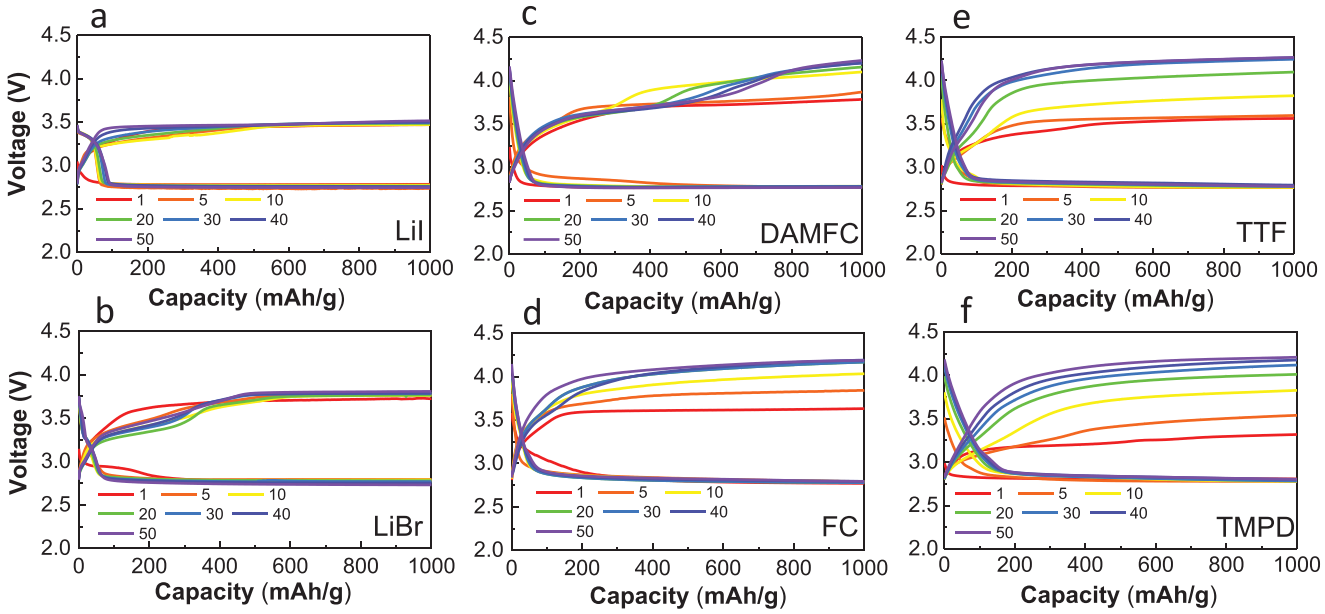

Figure 4. Galvanostatic cycling of Li–O_2 battery using selected "primary" RMs in 1 M LiTFSI dissolved in DMSO as the electrolyte. They are a) LiI and b) LiBr from halides, c) DAMFC and d) FC from organometallics, and e) TTF and f) TMPD from organics. The batteries are tested with limited capacity at 1000 mAh g^{-1}.

However, overpotential and curve configuration of organometallic RMs in TEGDME exhibit different trends than those of the DMSO electrolyte. The FC and DAMFC with TEGDME electrolyte revealed lower charge potentials (both at 3.4 V) for the 1st cycle compared to DMSO (3.6 V for FC and 3.9 V for DAMFC). In addition, the rate of increase in the cell overpotential in TEGDME electrolyte was faster than in DMSO, as the cell with FC in TEGDME took only 5 cycles to increase from 3.4 to 4.2 V, whereas it ran until 20th cycle to get its charge potential to increase from 3.6 to 4.2 V in DMSO electrolyte. When it comes to the halide group, however, there are tremendous differences in terms of charge–discharge profiles for both LiI and LiBr in DMSO and TEGDME (see Figures 4a,b and 5a,b). For example, while consistent overpotentials were recorded for both halides in DMSO electrolyte, elevated charge potentials along with a second plateau were observed in TEGDME, which is associated with the undesired X_3^-/X_2 redox couple.[26] As a polar solvent, DMSO with its higher Gutmann acceptor number

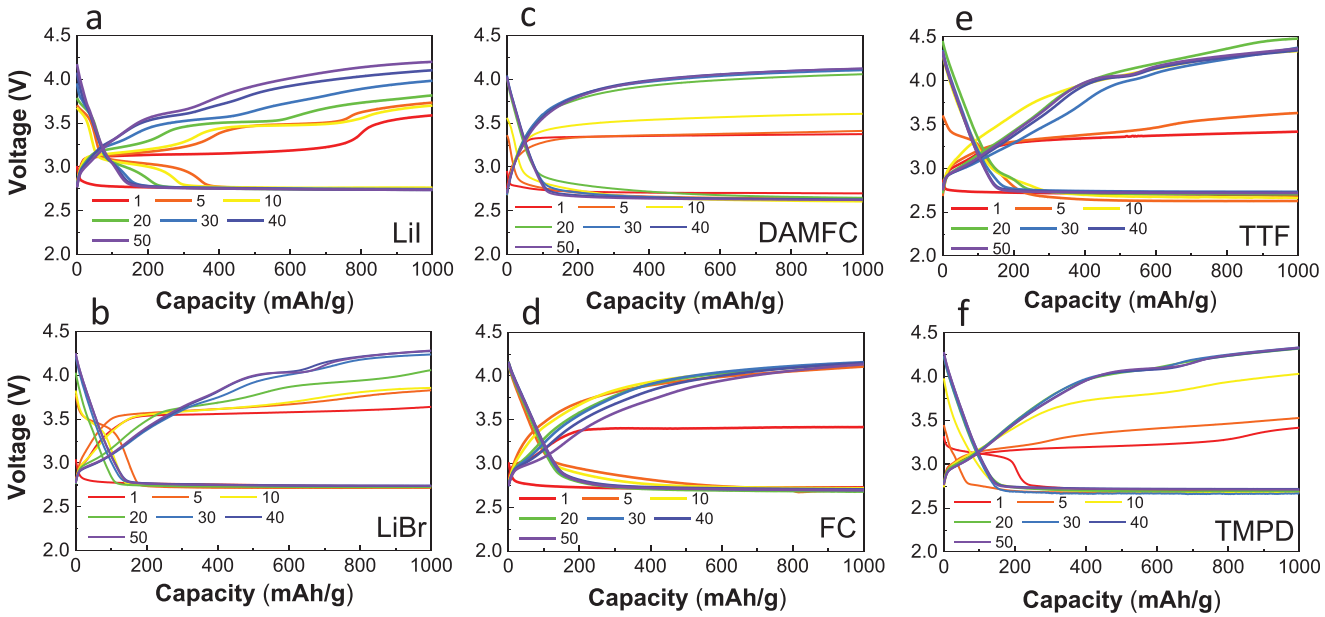

Figure 5. Galvanostatic cycling of Li–O_2 battery using selected "primary" RMs in 1 M LiTFSI dissolved in TEGDME as the electrolyte. They are a) LiI and b) LiBr from halides, c) DAMFC and d) FC from organometallics, and e) TTF and f) TMPD from organics. The batteries are tested with limited capacity at 1000 mAh g^{-1}.

(AN)[43] can better stabilize I^-/I_3^-, so that I^- does not go to its highest oxidized form (I_2) for assisting the oxidation of Li_2O_2. However, in the case of TEGDME with lower AN number,[44] it is more preferred to stabilize molecular Iodine (I_2) than its ions (I^- or I_3^-).[45,46] I^- can then facilitate the second step during charge, that is to its highest oxidation state (I_2) but not I_3^- like in DMSO. Because I_2 has no charge, it is not preferred to move within the electrolyte, and the I^- to I_2 ratio next to the cathode is then expected to decrease with increasing number of cycles, resulting in the elevated charge potential after each cycle. In addition, we noticed that the first plateau associated with I^-/I_3^- ($I^- \rightarrow I_3^- + e^-$) shows lower potential in TEGDME than in DMSO. This can be explained by considering the Nernst equation (see Equation (3)). During charge, the half-cell oxidation potential variance, ΔE_{Oxi}, is determined by the concentration of I^- (reduced form, α_{red})/I_3^- (oxidized form, α_{oxi}) ratio. The higher the ratio is, the lower is the charge potential. Since the partial concentration of I_3^- in TEGDME is consumed to form I_2, thus I^-/I_3^- ratio becomes higher than in DMSO (no I_2 formation), resulting in lower charge potential.

$$\Delta E_{Oxi} = -(RT/nF)\ln(\alpha_{Red}/\alpha_{Oxi}) \quad (3)$$

Recently, the parasitic reactions such as redox shuttling effect were reported for un-protected anodes during the charging of the Li–O_2 batteries with redox mediators.[47,48] However, as shown by Nakanishi et al.,[26] the shuttling effect can be prohibited if the mediated reactions between Li_2O_2 and RM* (reduced form of RM) are significantly faster than the diffusion rates of RM* toward the anode side. We argue that even though anode protection was not involved in this study, with moderate current density (0.5 A g^{-1}) and low concentration of each RM (20×10^{-3} M), our results are rationally representative for a redox-mediated effect associated with Li_2O_2 formation (see Section S4 in the Supporting Information). This is further confirmed by our results shown in Figures 4 and 5, as there is no evidence for the redox shuttling effect during discharge and charge processes. We note that it is possible to observe redox shuttling effect at higher cycles, however, the conclusion of this paper is valid for the tested 50 cycles using relatively lower RM concentrations and moderate current density of 0.5 A g^{-1}.

2.4. Computational Studies

We carried out DFT calculations to further understand the experimental results for the studied organic RMs. All the geometries of the RMs, that are of interest in this paper, were optimized in vacuum at the B3LYP/6-31G* level of theory[49,50] using the Gaussian16 code[51] except in case of LiI, where I atom was treated with the def2svp[52] basis set. These optimized geometries were then subjected to single point computations at the B3LYP/6-31+G* level (except in case of I atom, where def2svp basis set was used) using the Solvation Model based on Density (SMD model).[53] Here, DMSO was selected as the solvent to be consistent with the experimental studies. Furthermore, to compute oxidation potentials, free energy calculations were performed as follows. Single point B3LYP/6-31+G*[54] calculations were performed on the optimized geometries to obtain the energies of RMs in solvents. Oxidation potentials are then computed by taking the absolute free energy difference between neutral species and corresponding cations and subtracting 1.24 V (the standard electrode potential of Li^+/Li^+) from those values. We note that calculations of the oxidation potentials with the ωB97-XD functional are in agreement with the B3LYP results for the oxidation potentials (see Section S8 in the Supporting Information).The computed B3LYP oxidation potentials for the organic RMs fall within the range of 2.7–3.9 eV with the trends in the calculated oxidation potentials being similar to experiment. There are slight differences in trends for the thiazine type of molecules and inorganic molecules. Overall, both experiment and theoretical results suggest that these molecules can serve as RMs due to their oxidation potential values that are below 3.9 eV, as seen in Figure S8 in the Supporting Information. The computed oxidation potentials of the redox mediators have listed in Table S2 in the Supporting Information and a more detailed description of these calculations is provided in Section S8 in the Supporting Information.

To further understand the reason behind their destabilization in batteries, we have performed simulations by testing the reaction of six RMs (LiI, LiBr, TTF, TMPD, FC, and DAMFC) with singlet and triplet O_2 molecules. We carried out our calculations at the B3LYP/6-31G* level of theory. Singlet oxygen energies were corrected by adding 0.98 eV to account for the DFT error in the singlet energy.[37] The optimized structures and transition states can be seen in **Table 1**. The lower reaction energy barriers between singlet oxygen and TTF compared to others, suggests decomposition is faster in case of TTF. Also, we observed that TTF prefers to undergo ene-type of reaction, which is consistent with the results by Kwak et al.[37] However, we also found that an additional stable TTF–O_2 complex can exist. In the case of TMPD, singlet oxygen prefers to undergo cycloaddition. In case of FC and DAMFC, we observed that singlet oxygen is bonded between the cyclopentadiene ring and Fe. In a different reaction, we found that singlet oxygen attacked at the N-site of the DAMFC molecule and this has the lowest reaction energy barrier. The optimized geometries of LiI and LiBr with singlet oxygen are shown in Table 1. As can be seen from the results in the table, the interaction of these two RMs is weak, so they will be very stable. In addition, we investigated: 1) the interactions of the RMs* (oxidized form of RMs, LiI_3, $LiBr_3$, TTF^+, $TMPD^+$, FC^+, and $DAMFC^+$) with singlet oxygen in Table S3 in the Supporting Information, and 2) the interactions of the RMs with triplet oxygen, shown in Table S4 in the Supporting Information. All these interactions were found to be comparatively weaker, with the exception of TTF^+ and singlet oxygen, and thus in most cases not likely to result in decomposition of the RM or RM*.

These results suggest that TTF, TMPD, FC, and DAMFC potentially decompose in the presence of singlet oxygen and hence lose their efficiency of being RMs at that point. This can be the main reason for experimental observation of such low number of battery cycles when these RMs were used. Contrary to this, singlet oxygen did not affect number of cycles in case of LiI or LiBr. This could be partly due to the weak interaction of LiX (X = Br, I) with O, which can be seen by these results.

Table 1. Free energy changes (in eV) for the reactions between LiI, LiBr, TTF, and TMPD with singlet oxygen. Also, barriers (in eV) for these reactions are given.

Description	RM	$RM + {}^1O_2$	ΔG	$\Delta G^{\ddagger}$
LiI			0.81	Not found
LiBr		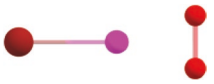	1.43	Not found
TMPD	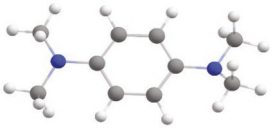	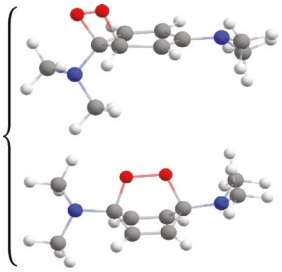	0.43 0.96	0.58 1.04
TTF	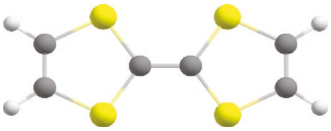	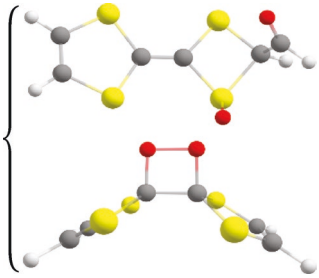	−2.37 −0.88	Not found 0.42
FC	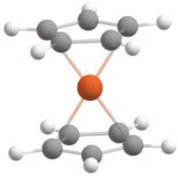	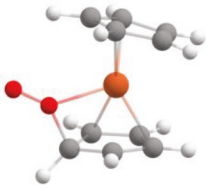	0.78	0.82
DAMFC	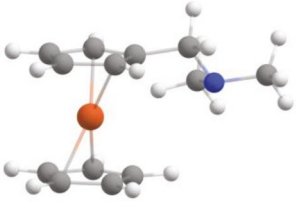	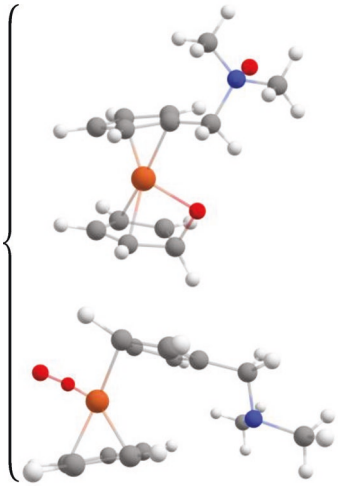	−0.29 0.30	0.31 0.33

3. Conclusions

In summary, we comprehensively reviewed 20 RMs via CV and galvanostatic cycling tests within identical conditions for their possible use as electrocatalysts in Li–O_2 batteries. Results show various responses of each RMs, where "primary RMs" were selected as more preferable choices than others in terms of their electrochemical characteristics and stabilities. The stability for tested RMs was found to follow the order of halides > organics > organometallics. Our results indicate that some organic and organometallic RMs such as TTF and FC reveal better effectiveness than halides for suppressing charge overpotentials during early stage, yet they show instabilities at higher cycles. Our DFT calculations suggest that in case of organic RMs, the reason for the observed instabilities could be due to their dissociation in presence of singlet oxygen, which can be liberated in the dissociation step of Li_2O_2. However, DFT calculations of LiI or LiBr reactions with singlet oxygen did not give any significant change in the bond length of oxygen nor there was any strong bond between Li and O. This indicates that LiI and LiBr are not susceptible to singlet oxygen. This study provides a new insight into the activity and stability of different classes of RMs.

4. Experimental Section

CV: CV experiments were performed in a single compartment three-electrode setup. A platinum wire[26,55] with a surface area of 0.4 cm^2 was used as working electrode and Li foil as counter electrode. An Ag/Ag^+ was used as a reference electrode (Section S3, Supporting Information). 1 M LiTFSI was used as a salt. The experiments were performed with 20×10^{-3} M of RMs in 3 mL of DMSO and TEGDME solvent at the scan rate of 10 mV s^{-1}. Each electrolyte was presaturated with both Ar and O_2 before test.

Cathode Preparation: The cathode for the battery experiments was fabricated by coating the carbon slurry on top of the air-permeable carbon paper (Sigracet GDL 35BC). The carbon slurry was made by blending carbon black powders (Ketjenblack EC-600JD) with a diluted organic binder (7 wt% polyvinylidene fluoride in *N*-methyl-2-pyrrolidone) and mixed for 5 min to make sure its uniformity. The slurry was then film coated on top of carbon paper and dried for 12 h in vacuum oven at 80 °C before use.

Battery Test: Two-compartment Swagelok cells were used for all Li–O_2 battery tests. The cells were assembled in an Ar-filled glovebox with both oxygen and humidity levels less than 0.1 ppm. The battery is composed of Li metal foil anode (MTI Corp), a porous glass-fiber separator (Whatman, GF/B), and as-prepared carbon paper cathode. A stainless mesh was attached to the back of the cathode and the hollow current collector in case of battery deformation during the assembly. A dehydration process was applied for both electrolytes (molecular sieves, 4 Å, Sigma-Aldrich, H_2O in electrolyte <20 ppm) and electrode (vacuum oven) to eliminate the parasitic side reactions. After assembly, the battery was then taken outside the glovebox and flowed with pure O_2 for 15 min. Battery tests were performed with a galvanostatic battery analyzer (MTI Corp, BST8-MA) at room temperature for a limited capacity of 1000 mAh g^{-1}.

Supporting Information

Supporting Information is available from the Wiley Online Library or from the author.

Acknowledgements

A.S.-K., C.Z., S.R., L.A.C, N.D., and A.T.N. acknowledge the support by the U.S. Department of Energy, Office of Energy Efficiency and Renewable Energy, Vehicle Technologies Office. S.N.M. acknowledges the support by the National Science Foundation (grant no. NSF-DMREF 1729420). The authors acknowledge a grant of computer time at the Argonne National Laboratory LCRC computer facility.

Conflict of Interest

The authors declare no conflict of interest.

Author Contributions

The experimental work was completed by A.S.-K., C.Z., S.N.M., and S.R.; characterization was done by C.Z., Z.H., and S.R.; and DFT calculations were performed by L.A.C., N.D., and A.T.N.

Keywords

cyclic voltammetry, density functional theory, Li–O_2 batteries, redox mediators

Received: January 17, 2020
Revised: May 3, 2020
Published online: June 5, 2020

[1] N. Imanishi, A. C. Luntz, P. Bruce, *The Lithium Air Battery: Fundamentals*, Vol. *XI*, Springer, Berlin **2014**, p. 318.
[2] A. C. Luntz, B. D. McCloskey, *Chem. Rev.* **2014**, *114*, 11721.
[3] D. Aurbach, B. D. McCloskey, L. F. Nazar, P. G. Bruce, *Nat. Energy* **2016**, *1*, 16128.
[4] B. D. McCloskey, C. M. Burke, J. E. Nichols, S. E. Renfrew, *Chem. Commun.* **2015**, *51*, 12701.
[5] Y. Cheng, H. J. Chang, H. Dong, D. Choi, V. L. Sprenkle, J. Liu, Y. Yao, G. Li, *J. Mater. Res.* **2016**, *31*, 3125.
[6] G. Girishkumar, B. McCloskey, A. C. Luntz, S. Swanson, W. Wilcke, *J. Phys. Chem. Lett.* **2010**, *1*, 2193.
[7] M. Asadi, B. Sayahpour, P. Abbasi, A. T. Ngo, K. Karis, J. R. Jokisaari, C. Liu, B. Narayanan, M. Gerard, P. Yasaei, X. Hu, A. Mukherjee, K. C. Lau, R. S. Assary, F. Khalili-Araghi, R. F. Klie, L. A. Curtiss, A. Salehi-Khojin, *Nature* **2018**, *555*, 502.
[8] B. D. McCloskey, R. Scheffler, A. Speidel, D. S. Bethune, R. M. Shelby, A. C. Luntz, *J. Am. Chem. Soc.* **2011**, *133*, 18038.
[9] B. D. McCloskey, D. S. Bethune, R. M. Shelby, G. Girishkumar, A. C. Luntz, *J. Phys. Chem. Lett.* **2011**, *2*, 1161.
[10] A. Kraytsberg, Y. Ein-Eli, *J. Power Sources* **2011**, *196*, 886.
[11] F.-L. Meng, Z.-W. Chang, J.-J. Xu, X.-B. Zhang, J.-M. Yan, *Mater. Horiz.* **2018**, *5*, 298.
[12] Z.-L. Wang, D. Xu, J.-J. Xu, L.-L. Zhang, X.-B. Zhang, *Adv. Funct. Mater.* **2012**, *22*, 3699.
[13] J.-J. Xu, Z.-W. Chang, Y. Wang, D.-P. Liu, Y. Zhang, X.-B. Zhang, *Adv. Mater.* **2016**, *28*, 9620.
[14] J.-J. Xu, Z.-W. Chang, Y.-B. Yin, X.-B. Zhang, *ACS Cent. Sci.* **2017**, *3*, 598.
[15] J.-J. Xu, Z. L. Wang, D. Xu, F. Z. Meng, X. B. Zhang, *Energy Environ. Sci.* **2014**, *7*, 2213.
[16] M. M. Ottakam Thotiyl, S. A. Freunberger, Z. Peng, Y. Chen, Z. Liu, P. G. Bruce, *Nat. Mater.* **2013**, *12*, 050.

[17] M. Asadi, B. Kumar, C. Liu, P. Phillips, P. Yasaei, A. Behranginia, P. Zapol, R. F. Klie, L. A. Curtiss, A. Salehi-Khojin, *ACS Nano* **2016**, *10*, 2167.
[18] L. Majidi, Z. Hemmat, R. E. Warburton, K. Kumar, A. Ahmadiparidari, L. Hong, J. Guo, P. Zapol, R. F. Klie, J. Cabana, J. Greeley, L. A. Curtiss, A. Salehi-Khojin, *Chem. Mater.* **2020**, *32*, 2764.
[19] A. Halder, A. T. Ngo, X. Luo, H.-H. Wang, J. G. Wen, P. Abbasi, M. Asadi, C. Zhang, D. Miller, D. Zhang, J. Lu, P. C. Redfern, K. C. Lau, R. Amine, R. S. Assary, Y. J. Lee, A. Salehi-Khojin, S. Vajda, K. Amine, L. A. Curtiss, *J. Phys. Chem. A* **2019**, *123*, 10047.
[20] J.-B. Park, S. H. Lee, H.-G. Jung, D. Aurbach, Y.-K. Sun, *Adv. Mater.* **2018**, *30*, 1704162.
[21] Z. Chang, J. Xu, X. Zhang, *Adv. Energy Mater.* **2017**, *7*, 1700875.
[22] Y. Ko, H. Park, B. Kim, J. S. Kim, K. Kang, *Trends Chem.* **2019**, *1*, 349.
[23] I. Landa-Medrano, I. Lozano, N. Ortiz-Vitoriano, I. Ruiz de Larramendi, T. Rojo, *J. Mater. Chem. A* **2019**, *7*, 8746.
[24] Z. Liang, Y.-C. Lu, *J. Am. Chem. Soc.* **2016**, *138*, 7574.
[25] Y. Chen, S. A. Freunberger, Z. Peng, O. Fontaine, P. G. Bruce, *Nat. Chem.* **2013**, *5*, 489.
[26] A. Nakanishi, M. L. Thomas, H.-M. Kwon, Y. Kobayashi, R. Tatara, K. Ueno, K. Dokko, M. Watanabe, *J. Phys. Chem. C* **2018**, *122*, 1522.
[27] R. Yu, W. Fan, X. Guo, S. Dong, *J. Power Sources* **2016**, *306*, 402.
[28] C. M. Burke, R. Black, I. R. Kochetkov, V. Giordani, D. Addison, L. F. Nazar, B. D. McCloskey, *ACS Energy Lett.* **2016**, *1*, 747.
[29] D. Kundu, R. Black, B. Adams, L. F. Nazar, *ACS Cent. Sci.* **2015**, *1*, 510.
[30] X. Gao, Y. Chen, L. R. Johnson, Z. P. Jovanov, P. G. Bruce, *Nat. Energy* **2017**, *2*, 17118.
[31] D. Sun, Y. Shen, W. Zhang, L. Yu, Z. Yi, W. Yin, D. Wang, Y. Huang, J. Wang, D. Wang, J. B. Goodenough, *J. Am. Chem. Soc.* **2014**, *136*, 8941.
[32] B. J. Bergner, C. Hofmann, A. Schürmann, D. Schröder, K. Peppler, P. R. Schreiner, J. Janek, *Phys. Chem. Chem. Phys.* **2015**, *17*, 31769.
[33] D. G. Kwabi, *M.Sc. Mech. Eng. Thesis*, Massachusetts Institute of Technology, Cambridge, MA **2013**.
[34] A. J. Bard, L. R. Faulkner, *Electrochemical Methods: Fundamentals and Applications*, 2nd ed. (Ed: D. Harris), John Wiley & Sons, Inc., New York **2001**.
[35] N. M. Elgrishi, K. J. Rountree, B. D. McCarthy, E. S. Rountree, T. T. Eisenhart, J. L. Dempsey, *J. Chem. Educ.* **2018**, *95*, 197.
[36] P. Zhang, Y. Zhao, X. Zhang, *Chem. Soc. Rev.* **2018**, *47*, 2921.
[37] W.-J. Kwak, H. Kim, Y. K. Petit, C. Leypold, T. T. Nguyen, N. Mahne, P. Redfern, L. A. Curtiss, H.-G. Jung, S. M. Borisov, S. A. Freunberger, Y.-K. Sun, *Nat. Commun.* **2019**, *10*, 1380.
[38] W.-J. Kwak, H. Kim, H.-G. Jung, D. Aurbach, Y.-K. Sun, *J. Electrochem. Soc.* **2018**, *165*, A2274.
[39] A. C. Luntz, B. D. McCloskey, *Chem. Rev.* **2014**, *114*, 11721.
[40] B. D. McCloskey, A. Valery, A. C. Luntz, S. R. Gowda, G. M. Wallraff, J. M. Garcia, T. Mori, L. E. Krupp, *J. Phys. Chem. Lett.* **2013**, *4*, 2989.
[41] N. Mahne, O. Fontaine, M. O. Thotiyl, M. Wilkening, S. A. Freunberger, *Chem. Sci.* **2017**, *8*, 6716.
[42] N. Mahne, B. Schafzahl, C. Leypold, M. Leypold, S. Grumm, A. Leitgeb, G. A. Strohmeier, M. Wilkening, O. Fontaine, D. Kramer, C. Slugovc, S. M. Borisov, S. A. Freunberger, *Nat. Energy* **2017**, *2*, 17036.
[43] U. Mayer, V. Gutmann, W. Gerger, *Monatsh. Chem.* **1975**, *106*, 1235.
[44] F. Cataldo, *Eur. Chem. Bull.* **2015**, *4*, 92.
[45] G. M. Loudon, *Organic Chemistry*, Oxford University Press, Oxford **2003**, p. 317.
[46] V. Gold, *Pure Appl. Chem.* **1979**, *51*, 1725.
[47] N. Feng, P. He, H. Zhou, *ChemSusChem* **2015**, *8*, 600.
[48] B. J. Bergner, M. R. Busche, R. Pinedo, B. B. Berkes, D. Schröder, J. Janek, *ACS Appl. Mater. Interfaces* **2016**, *8*, 7756.
[49] A. D. Becke, *J. Chem. Phys.* **1993**, *98*, 1372.
[50] C. T. Lee, W. T. Yang, R. G. Parr, *Phys. Rev. B* **1988**, *37*, 785.
[51] M. J. Frisch, G. W. Trucks, H. B. Schlegel, G. E. Scuseria, M. A. Robb, J. R. Cheeseman, G. Scalmani, V. Barone, G. A. Petersson, H. Nakatsuji, X. Li, M. Caricato, A. V. Marenich, J. Bloino, B. G. Janesko, R. Gomperts, B. Mennucci, H. P. Hratchian, J. V. Ortiz, A. F. Izmaylov, J. L. Sonnenberg, D. Williams-Young, F. Ding, F. Lipparini, F. Egidi, J. Goings, B. Peng, A. Petrone, T. Henderson, D. Ranasinghe, *Gaussian 16, Revision C.01*, Gaussian, Inc., Wallingford, CT **2016**.
[52] J. Zheng, X. Xu, D. G. Truhlar, *Theor. Chem. Acc.* **2011**, *128*, 295.
[53] J. Tomasi, B. Mennucci, R. Cammi, *Chem. Rev.* **2005**, *105*, 2999.
[54] A. D. Becke, *J. Chem. Phys.* **1993**, *98*, 5648.
[55] G. Leverick, M. Tułodziecki, R. Tatara, F. Bardé, Y. Shao-Horn, *Joule* **2019**, *3*, 1106.

